BMC Chemistry

RESEARCH

Open Access

Computational and experimental insights into the spectroscopy, electronic states, and molecular docking of (2*S*)-2,6-diaminohexanoic acid [DAHA]

T. Amna Sherin[1†], P. V. Abdul Nazar[1], Sandhya Savita[1,2†], Mudassar Shahid[3], Nazia Siddiqui[4*] and Saleem Javed[1*]

Abstract

This paper presents a theoretical analysis of the L-Lysine molecule using the DFT (density functional theory) method with a 6-311++G(d,p) basis set, a quantum–mechanical atomistic simulation method. The research encompasses the analysis of optimized chemical structure, vibrations, FMO, ELF, NLO, RDG, etc., to study the molecule's intensive properties, stability, and other biological activities. IR and UV spectra were analysed for the spectrochemical study, and the VEDA program was used to determine the PED values. The chemical reactivity of the molecule was identified through analysis of the Frontier molecular orbitals, Fukui, and molecular electrostatic potential. The electron localization function and reduced density gradient were determined to understand bonding and electronic structure. The temperature dependence on the properties of the molecule was estimated. The optical properties of the molecule were discussed by analyzing the non-linear optical property. The feasibility of the molecule as a therapeutic drug was examined using the drug likeness concept. Molecular docking analysis was conducted to acquire the best ligand–receptor complex and to study the molecule's biological activity.

Keywords DFT, MEP, ELF, Molecular docking, RDG

Introduction

L-lysine is an essential α-amino acid required for protein synthesis and various physiological processes. It plays a critical role as a precursor for proteins and contributes to numerous health benefits, including collagen formation, antibody production, enzyme and hormone synthesis, anxiety relief, surgery recovery, and muscle protein building [1]. As the human body cannot produce lysine, it must be obtained through diet. However, lysine deficiency leads to several disease states, such as anemia, connective tissue defects, protein-energy malnutrition, and metabolic disorders [2–4]. Despite its well-known biological significance, there remains a need to explore its multifunctionality and diverse applications in industrial and medicinal fields. In particular, lysine's growing role in biotechnology, and

†T. Amna Sherin and Sandhya Savita have equal authorship.

*Correspondence:
Nazia Siddiqui
dr.naazsiddiqui@gmail.com
Saleem Javed
saleem.7javed@gmail.com
[1] Department of Chemistry, Jamia Millia Islamia, New Delhi 110025, Delhi, India
[2] Guru Ghasidas Vishwavidyalaya, Bilaspur 495009, Chhattisgarh, India
[3] Department of Pharmaceutics, College of Pharmacy, King Saud University, 11451 Riyadh, Saudi Arabia
[4] Department of Chemistry, Dayalbagh Educational Institute, Agra 282005, Uttar Pradesh, India

nanotechnology, and its potential to enhance health outcomes remains underexplored. This study investigates the structural and functional aspects of lysine, focusing on its role in health, metabolism, and emerging applications in nanotechnology and biomaterials. The purpose of this work is to bridge the gap between lysine's essential biological functions and its broader applications, which could have significant implications in medicine and industry.

The chemical structure of lysine, or L-Lysine (commonly referred to as (2*S*)-2,6-diaminohexanoic acid [DAHA]), is C6H14N2O2. This aliphatic compound consists of a protonated amine group (NH_3^+), a carboxylic group (COO–), and a lysyl side chain ((CH2)4NH2). DAHA is symbolized as Lys or K and is a positively charged, dibasic amino acid due to its second primary amino group. These unique structural features allow DAHA to participate in intermolecular charge transfer, giving it distinct functional properties. The lysyl side chain differentiates DAHA from other amino acids, contributing to its biological and biochemical roles. Notably, lysine is abundant in histones, essential proteins for DNA packaging, with lysine-rich variants such as H1, H2A, and H2B [5].

Historically, Heinrich Drechsel, a German chemist, first isolated DAHA from casein [6]. DAHA is synthesized industrially as monohydrochloride (DAHA-HCl) through fermentation using Corynebacterium, followed by HCl neutralization and crystallization. Alternatively, fluidized bed granulation can synthesize it as carbonate granules, where carbon dioxide produced during fermentation neutralizes the DAHA solution [7].

Metabolically, DAHA is converted into acetyl-CoA, an essential intermediate for ATP production. Its derivative, allysine, is a key component in synthesizing collagen and elastin, critical for connective tissue integrity [8]. DAHA supplements are widely used to reduce the frequency of cold sore outbreaks by controlling the herpes simplex virus (HSV) [9]. Beyond its health benefits, lysine has emerging applications in industrial and technological fields. For example, DAHA's role as a crystal growth inhibitor is being explored in producing nano zeolites, an area of growing industrial importance. Furthermore, combining DAHA with L-arginine enhances collagen production and bone-forming cell activity, demonstrating its relevance in bone health and regenerative medicine. The findings highlight lysine's significant potential in traditional health supplements and advanced fields such as tissue engineering and nanomaterials. In athletics, DAHA is a protein supplement aiding muscle recovery after stress. These findings highlight lysine's multifunctionality and its significance in industrial chemistry, medicinal chemistry, and cosmetics [10–12].

Studies on DAHA remain limited, leaving many of its valuable properties unexplored. This work investigates DAHA's molecular characteristics using quantum chemical methods, integrating theoretical and experimental analyses such as FTIR and UV–Vis spectroscopy. Computational calculations were conducted to analyze its structure, with docking assays assessing its potential as a drug candidate or precursor. Key properties were explored and compared with experimental results, including vibrational modes, NLO, MEP, ELF, FMO, and thermodynamic variables. The study provides a comprehensive understanding of DAHA's characteristics and builds upon recent studies examining biologically active compounds, their structures, spectral data, and pharmacological potential [13–20].

Experimental details

A Perkin Elmer Spectrum FTIR instrument with a KBr beam splitter obtained FTIR spectra for solid-state DAHA in the 4000–550 cm^{-1} range. Using methanol as the solvent, a UV-1280 multifunctional spectrometer encompassing the ultraviolet range of 200–800 nm was used for UV–Visible analysis.

Computational methods

Density functional theory (DFT) is a crucial component of contemporary theoretical physics and a tool for characterizing molecules. The current study employs GaussView 5.0 and Gaussian 09W [21] to calculate the quantum chemical parameters. The B3LYP functional and the 6-311++G(d,p) basis set were used to determine the optimal geometry corresponding to the lowest energy [22, 23]. The optimized structure was used to analyze the molecular structural parameters, wave numbers, and highest occupied molecular orbital-lowest unoccupied molecular orbital, Non-Linear Optical, and Frontier Molecular Orbital Analysis. The VEDA program calculated the vibrational PED (potential energy distribution) [24]. The scaling factor of 0.9614 was applied to the frequencies to calculate the vibrational spectra of the molecule accurately [25]. TD-DFT method with the mentioned basis set was utilized to study the UV–Vis in the gaseous phase. All graphs and figures were created using Origin8.0 software and Multiwfn programs [26, 27]. The Atomistica thermo online tool provides the thermodynamic properties of the molecule. The swiss ADME program [28] analyzed the molecule's drug similarity and ADME characteristics. Molecular docking was examined using Autodock-Vina, and the interactive visualization and docking results were analysed using the UCSF Chimera program [29]. Koopman's theorem [30] was utilised to calculate the ionisation potential (IP) and the electron affinity (EA), i.e., $EA = -E_{LUMO}$ And $IP = -E_{HOMO.}$

Result and discussion

Optimized molecular geometry

DFT, B3LYP attained the equilibrium molecular structure of the DAHA and the basis set 6-311++G(d,p). DAHA is a neutral molecule with a single spin, a C1 point group, and a dipole moment of 5.8381 Debye. Table 1 presents the optimized bond lengths (BL) and bond angles (BA) of DAHA, as listed in Table 2. These values were determined experimentally from the CIF file [31] and theoretically using B3LYP/6-311++G(d,p), B3LYP/6-31+G(d), B3LYP-D3, and CAM-B3LYP, analyzing 22 BL and 39 BA. Figure 1 shows the optimized structure of DAHA. It is an aliphatic compound with two amino groups and a carboxylic acid group. It follows a linear structure. The DAHA molecule has 2 N–C, 5 C–C, 2 C–O, 4 N–H, and 9 C–H bonds. All C–C bonds have similar lengths and are also closely proximate to the exact C–C BL (1.54 Å). Among all the C–C bonds, the C1–C2 bond that binds to the most electronegative oxygen atom has the more considerable bond length (1.547 Å). The C1–O3 has a bond length of 1.203 Å, which indicates the presence of a double bond, whereas C1–O4 has a BL of 1.339 Å, which is more remarkable since the OH group is present, suggesting that there is a single bond. All the C–H bond lengths are almost equal. Among all these, the C17–H20 bond has a slighter higher BL (1.1 Å). This is due to the electron-releasing amino group, which induces an electron cloud and causes a longer bond length of nearer C–H bond. C–N bonds in the DAHA are almost equal in length and close to the exact value (1.47 Å). All four N–H bonds are practically equal and around 1 Å. CAM-B3LYP demonstrates the best agreement with experimental values, accurately predicting key bond angles (C2–C1–O3, O3–C1–O4) and bond lengths (C1–C2, C1–O3, C1–O4). B3LYP-D3 effectively accounts for dispersion, while B3LYP/6-311++G(d,p) and B3LYP/6-31+G(d) follow similar reliable trends. Overall, CAM-B3LYP provides the highest accuracy in reproducing molecular geometry. As the DAHA molecule is linear and has a flexible side chain, the steric hindrance is generally minimal compared to the amino acids with bulkier side chains. There was a significant correlation between the computed results and experimental results.

Vibrational studies

DAHA is a linear molecule with 24 atoms, producing 66 possible vibrational modes. The theoretically and experimentally recorded IR spectra are depicted in Fig. 2a, b. The Multiwfn program was used to plot the spectra. Table ST1 lists experimental wave numbers, computed

Table 1 Optimized geometrical bond lengths of DAHA

Parameter	B3LYP/6-311++G(d,p)	B3LYP/6-31+G(d)	B3LYP-D3	CAM-B3LYP	Experimental
Bond length (Å)					
C1–C2	1.55	1.55	1.55	1.54	1.53
C1–O3	1.20	1.21	1.20	1.20	1.25
C1–O4	1.34	1.34	1.34	1.33	1.25
C2–N7	1.48	1.48	1.48	1.47	1.48
C2–H6	1.09	1.09	1.09	1.09	0.91
N7–H11	1.01	1.02	1.02	1.01	1.01
N7–H12	1.02	1.02	1.02	1.01	0.89
C2–C5	1.54	1.54	1.53	1.53	1.52
C5–H9	1.10	1.10	1.10	1.09	1.06
C5–H10	1.09	1.10	1.09	1.09	1.09
C5–C8	1.53	1.53	1.53	1.52	1.52
C8–H15	1.09	1.10	1.09	1.09	1.11
C8–H16	1.09	1.10	1.09	1.09	1.02
C8–C14	1.53	1.53	1.53	1.53	1.53
C14–H18	1.09	1.10	1.10	1.09	1.18
C14–H19	1.09	1.09	1.09	1.09	1.07
C14–C17	1.53	1.53	1.53	1.53	1.52
C17–H20	1.10	1.11	1.10	1.10	1.04
C17–H21	1.09	1.09	1.09	1.09	1.04
C17–N22	1.47	1.47	1.47	1.46	1.48
N22–H23	1.02	1.02	1.02	1.01	0.82
N22–H24	1.01	1.02	1.01	1.01	0.97

Table 2 Optimized bond angles of DAHA

Parameter	B3LYP/6-311++G	B3LYP/6-31+G(d)	B3LYP-D3	CAM-B3LYP	Experimental
Bond angle (°)					
C2–C1–O3	122.99	122.89	122.89	122.84	116.74
C2–C1–O4	114.01	114.20	114.07	114.03	117.73
O3–C1–O4	122.98	122.88	123.01	123.11	125.49
C1–C2–C5	111.04	111.06	110.99	110.84	109.79
C1–C2–H6	104.47	104.89	104.47	104.57	117.31
C1–C2–N7	109.39	109.13	109.48	109.49	109.72
C5–C2–H6	108.69	108.78	108.74	108.72	103.87
C5–C2–N7	115.17	115.10	115.06	114.93	111.75
H6–C2–N7	107.48	107.29	107.51	107.73	104.24
C2–C5–C8	113.81	113.29	113.38	113.59	114.64
C2–C5–H9	108.59	108.66	108.61	108.65	106.06
C2–C5–H10	107.82	108.09	108.04	107.86	108.98
C8–C5–H9	109.99	109.96	110.01	110.01	115.66
C8–C5–H10	110.12	110.30	110.30	110.23	103.51
H9–C5–H10	106.22	106.25	106.24	106.22	107.68
C2–N7–H11	112.49	112.15	112.29	112.81	108.48
C2–N7–H12	111.54	111.12	111.31	111.79	103.52
H11–N7–H12	107.77	107.33	107.66	108.65	123.97
C5–C8–C14	112.88	112.69	112.29	112.75	110.99
C5–C8–H15	110.08	109.05	109.98	110.09	116.72
C5–C8–H16	108.92	109.05	109.01	108.08	113.53
C14–C8–H15	108.97	108.99	109.01	108.99	105.00
C14–C8–H16	109.55	109.62	109.63	109.56	108.28
H15–C8–H16	106.24	106.28	106.26	106.26	101.47
C8–C14–C17	113.26	113.02	113.07	113.12	111.56
C8–C14–H18	109.24	109.21	109.25	109.12	109.69
C8–C14–H19	110.17	110.14	110.13	110.24	116.43
C17–C14–H18	109.10	109.23	109.25	109.12	104.89
C17–C14–H19	108.49	108.59	108.62	108.49	105.19
H18–C14–H19	106.35	106.42	106.39	106.36	108.37
C14–C17–H20	109.07	109.05	108.97	109.06	114.35
C14–C17–H21	109.27	109.26	109.19	109.20	112.13
C14–C17–N22	110.71	110.58	110.66	110.65	110.88
H20–C17–H21	106.68	106.75	106.68	106.71	97.84
H20–C17–N22	113.42	113.57	113.51	113.35	105.91
H21–C17–N22	107.54	107.47	107.68	107.72	115.06
C17–N22–H23	110.85	110.58	110.77	111.22	107.25
C17–N22–H24	111.17	111.01	111.25	111.67	108.39
H23–N22–H24	107.11	106.91	107.14	107.61	96.62

harmonic oscillator wave numbers, IR intensities, and the PED assignment values of the DAHA molecule [32, 33]. The computed vibrational modes distributions were obtained through the B3LYP/6-311++G and VEDA program. It includes both the scaled and unscaled data of theoretical calculations. Stretching frequencies, in-plane and out-plane bending frequencies and torsional vibrations are symbolised as ν, β, and τ, respectively [34]. To minimise the unscaled wave number, a scaling factor of 0.961 is multiplied by the unscaled values. The distribution of vibrational modes is given in descending order. PED assignments show 23 stretching, 22 bending, and 21 torsional vibration modes. The experimental FT-IR values were determined in the solid phase of the molecule,

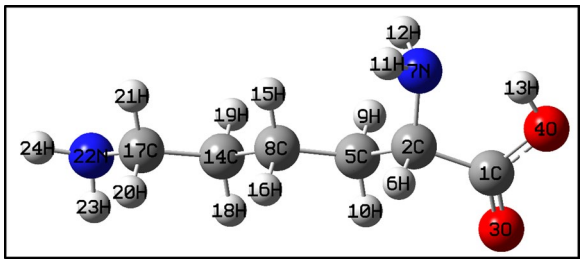

Fig. 1 Optimized structure of the DAHA molecule in the gas phase at the 6-311++G(d,p) level of theory

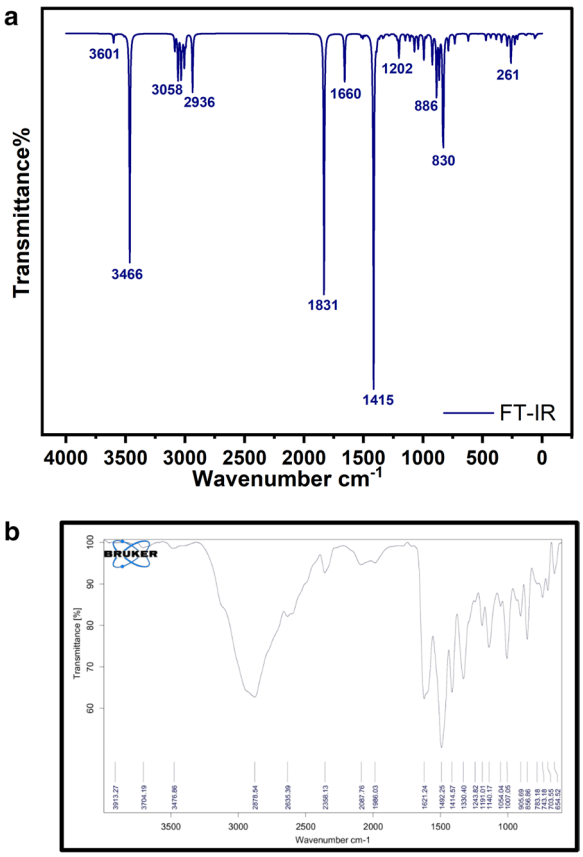

Fig. 2 **a** Theoretical FT-IR spectrum, **b** Experimental Infrared spectra of DAHA

and the graph was plotted using the FT-IR instrument. For both experimental and theoretical FT-IR, the R^2 value is 0.999, which shows a strong correlation between both values. Some of the significant vibrations are given below.

NH_2 group vibrations

In DAHA, the two NH_2 groups exhibit N–H IR vibrations: one involves stretching the N–H bonds, and the other consists in bending the H–N–H bonds. NH_2 group possesses three characteristic absorption bands in IR. Two are stretching vibrations, which affect symmetric and antisymmetric stretching with frequencies of 3300 cm^{-1} and 3500 cm^{-1}, respectively. One is the bending vibration mode with frequencies of 1590–1650 cm^{-1} [35]. Theoretical frequencies were computed using B3LYP/6-311++G, and the IR spectra were acquired through the Multiwfn program. According to the calculated values, N–H bonds show a stretching band at 3460 cm^{-1}, 3437 cm^{-1}, 3376 cm^{-1} and 3361 cm^{-1}. Vibrations at 3437 cm^{-1} and 3361 cm^{-1} have a theoretical PED contribution of 99%. The table shows that the intensity of IR is zero at 3437 cm^{-1}, 3376 cm^{-1}, and 3361 cm^{-1}. A peak at 3460 cm^{-1} is shown in the IR spectra. H–N–H bending vibrations are computed at 1596 cm^{-1} and 1593 cm^{-1} with 75% and 78% of PED contributions. An intense peak is observed at these wave numbers in the IR spectra. N–H bonds' torsional vibrations are obtained computationally at 282 cm^{-1} and 25 cm^{-1}.

COOH group vibrations

The DAHA exhibits an acid group in its linear structure, contributing to some peaks in the IR spectra. The carbonyl group is affected by substituting the neighbouring group, whose electrical and physical properties and conjugation [36]. The acid group vibrations consist of stretching and bending modes of O–H, C=O, and C–O bonds. Generally, Carboxylic acid O–H stretch shows a robust and comprehensive band at 3300 cm^{-1}–2500 cm^{-1}, and O–H bend is observed at 1440–1395 cm^{-1}. The absorption pattern observed at this peak is sharp and broad but will superimpose upon the sharp C-H stretching bands. Hence, they are indistinguishable from each other. The B3LYP/6-311++G computed theoretical calculation lists a stretching vibration at 3330 cm^{-1} with a theoretical PED contribution of 97%. The bend vibration of C–O–H shows a band at 1360 cm^{-1} with a PED value of 74%, the carbonyl C=O stretch generally occurs at 1760–1690 cm^{-1}, and the C–O stretch is obtained at 1320–1210 cm^{-1}. The theoretical calculations give a frequency of 1761 cm^{-1}, which indicates the stretching of C=O. The PED contribution of this stretching is 87%. Similarly, a Stretch of C–O is obtained at a frequency of 1156 cm^{-1} with 47% PED contribution. In-plane and out-of-plane bending modes of OCO vibrations are too weak 705 cm^{-1}. The bands of these stretching are more evident in the FT-IR plots.

CH and CH_2 vibrations

Typically, C-H bond stretching is noticed between 2800 and 3300 cm^{-1}. This band frequency also varies in alkane, alkene, and alkyne. The DAHA molecule has 9 C–H

bonds, showing peaks in the IR spectra. The calculated vibrational bands for C-H stretching are 2966 cm^{-1}, 2940 cm^{-1}, 2916 cm^{-1}, 2915 cm^{-1}, 2905 cm^{-1}, 2890 cm^{-1}, 2883 cm^{-1}, 2877 cm^{-1} and 2823 cm^{-1}. The vibrational band for HCH bending was formed at 1461 cm^{-1}, 1447 cm^{-1}, 1433 cm^{-1} and 1430 cm^{-1}.

CC vibrations

Generally, CC vibrations are seen at 1300–800 cm^{-1}. Theoretical stretching vibrational bands for C–C stretching are 1018 cm^{-1}, 1001 cm^{-1}, and 935 cm^{-1} with a PED value of 40%, 32%, and 25%, respectively. Bending vibrations of C–C–C bonds are theoretically perceived at 85 cm^{-1} with a PED value of 54%.

CN vibrations

The titled molecule has two CN bonds that exhibit stretching vibrations, resulting in peaks in the IR spectra. Generally, C–N single bonds possess a stretching frequency of 1200–1350 cm^{-1} [37]. Theoretical vibrational stretching bands are seen at 2823 cm^{-1}, 1068 cm^{-1}, 1048 cm^{-1} and 1031 cm^{-1}. The bending vibrational frequency of the H-N–C bond is 1371 cm^{-1} with a PED value of 120%.

UV spectra and frontier molecular orbital analysis

The UV spectra of the DAHA were recorded experimentally in methanol and estimated theoretically in gaseous form, DMSO, and methanol. The theoretical assessment was done using TD-DFT by the B3LYP method, and the -311++G (d, p) basis set was utilized with PCM (polarizable continuum solvation model). The combined spectra of UV DAHA molecules in different solvents are depicted in Fig. 3a, and the experimentally portrayed spectra are shown in Fig. 3b. Experimentally, the maximum photon absorption in methanol is observed at a wavelength (λmax) of 256 nm, while computational calculations show peaks at 221 nm in DMSO and methanol and 229 nm in the gaseous phase. These results indicate minimal changes in absorption peaks across solvents.

The slight variations in λmax arise from differences in solvent polarity and solute–solvent interactions. Methanol, a polar protic solvent, stabilizes the excited states more effectively than DMSO (polar aprotic) or the gaseous phase, leading to minor shifts in absorption wavelengths. This highlights the limited solvent sensitivity of the molecule's absorption behavior despite the stabilizing effects of solvents on electronic transitions. The $\lambda_{max,}$ Band gap, Excitation energy, and oscillatory strength with the different HOMO→LUMO transition in percentage were demonstrated in Table 3. The highest transition is shown by those with more oscillatory strength values [38, 39]. By using FMO analysis, the Compound's other reactivity and chemical stability can be ascertained [40].

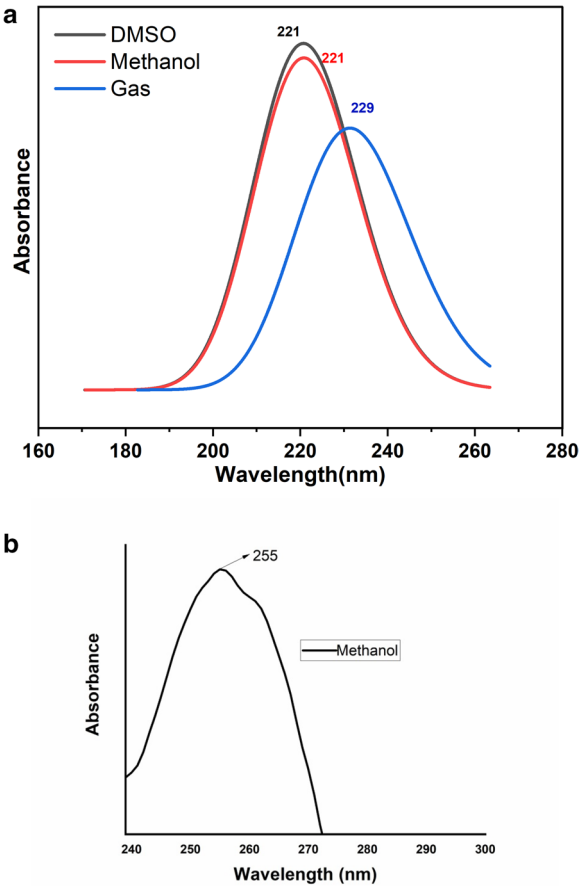

Fig. 3 **a** Combined UV–visible spectra, theoretical-gas phase, DMSO, and methanol, **b** experimental-methanol of DAHA molecule

FMO study is used to understand the reactiveness and stability of molecules. It consists of the analysis of the HOMO and LUMO, which will act as nucleophilic and electrophilic regions of molecules, respectively. The HOMO and LUMO energy gap are the lowest energy possessed by the electrons in a molecule. It determines the compounds' stability, chemical activity, molecules' colour, and other characteristics [41, 42]. Figure 4 shows the HOMO (− 5.347 eV) and LUMO (− 1.756 eV) diagram of the DAHA molecule, with a HOMO–LUMO energy gap of 3.591 eV. The HOMO is predominantly around the NH_2 attached to the C17 carbon. The red part denotes the positive region, and the green indicates the negative area. The LUMO is predominantly around the COOH group and NH_2 group attached to the C_2 carbon. The HOMO–LUMO energy gap can compute ionization energy, electro negativity, electron affinity, chemical hardness and softness, and chemical potential shows the DAHA molecule's computed properties: the ionisation

Table 3 Comparison of electronic properties of DAHA attained experimentally and calculated by TD-DFT/B3LYP method

Solvents	Experimental	TD-DFT B3LYP /6-311++G(d,p)				
	Wavelength λ_{max} (nm)	Wavelength λ_{max} (nm)	Band gap (eV)	Energy (cm^{-1})	Oscillatory strength (f)	Assignments
Gas	–	204	6.08	49061.87	0.01	H→L+2(91%)
		229	5.38	43356.31	0.01	H→L+1(68%)
		211	5.89	47474.58	0.01	H-1→L(41%)
DMSO	–	221	5.61	45217.84	0.02	H→L+1(75%)
		196	6.31	50928.24	0.01	H→L+3(71%)
		198	6.27	50574.16	0.01	H→L+2(25%)
Methanol	256	221	5.61	45210.58	0.02	H→L+1(75%)
		196	6.31	50912.92	0.01	H→L+3(71%)
		198	6.27	50550.77	0.01	H→L+2(25%)

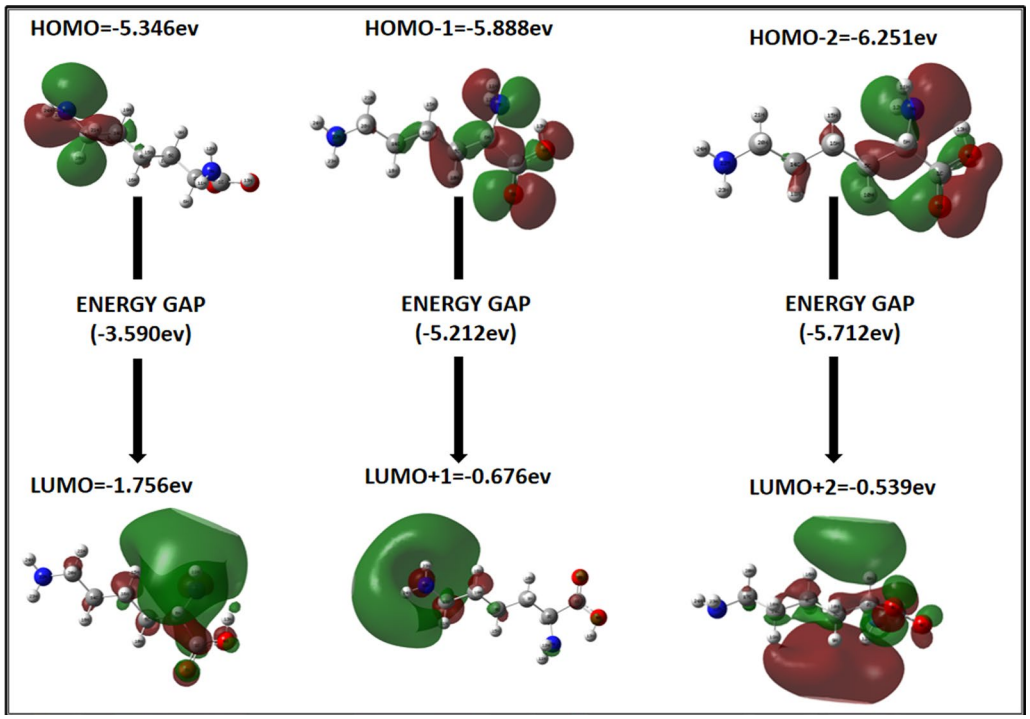

Fig. 4 HOMO-LUMO diagrams and bandgap energy of DAHA calculated using the 6-311++G(d,p) level of theory

potential is − 5.347 eV, the electron affinity is − 1.756 eV, the electronegativity is − 3.551 eV, and the chemical hardness is -1.795 eV. The value of chemical hardness and electronegativity gives molecules stability and biological characteristics. The electrophilicity index of the molecule, approximately − 3.512 eV, characterizes its electrophilic nature and suggests its potential bioactivity [43]. The chemical softness of the molecule, being significantly low at − 0.557 eV, implies the non-toxic nature of the DAHA molecule (Shown in Table 4).

From these values, Chemical reactivity descriptors were procured using the formula,

$$\text{Electronegativity}(\chi) = \text{HOMO} + \text{LUMO}/2,$$

$$\text{Chemical potential}(\mu) = -(\text{HOMO} + \text{LUMO})/2,$$

$$\text{Chemical hardness}(\eta) = (\text{HOMO}-\text{LUMO})/2,$$

$$\text{Chemical softness}(\sigma) = 1/\eta,$$

$$\text{Electrophilicity index } (\omega) = \chi^2/2\eta.$$

Electron localization function (ELF) and localized orbital locator (LOL)

The ELF quantifies the chance of locating the same spin electron at a specific region concerning the reference electron [44]. It is a method for assessing the probability of electron pairs in a multi-electronic system and the extent of spatial localization of the standard electron. The localized electrons are those confined to a specific region within the molecule. The nature of electrons in nuclear systems can be qualitatively understood using this technique. ELF, rooted in Pauling's repulsion principle, suggests that similar particles in the same space will repel each other, with values from 0 to 1 [45]. ELF value of 1 shows the most intense Pauling repulsion, where localized electrons are more concentrated and form a broad area in the ELF projection diagram. ELF value nearer to 0 indicates the space with minimum Pauling repulsion. This diagram helps us to understand molecules' stability, molecular bonding, chemical structure, resonance extension, and reactivity. Figure 5a is the 3D graphical representation of ELF values with a coloured map and surface map with a projection of the ELF of the DAHA molecule. In colour-filled maps, the Colour gradient shows the range of ELF values. The highest value is displayed in red, then orange, yellow, and green, while the lowest ELF value is visualized in blue. The region of the H-atom with a single electron is represented by the red area, indicating the highest Pauling repulsion. The oxygen-surrounded area is depicted in orange, where the repulsion is less and resonance occurs. The carbon and nitrogen-surrounded area is in blue, indicating minimum Pauling repulsion.

The surface map with projection is illustrated in Fig. 5b. The broad area on the map denotes the most localised electrons, and the narrow part of the figure shows the resonance or delocalised electrons. The high ELF value C–H covalent region indicates a substantial level of electron localization. The areas surrounding the valance and inner shell of C, N, and O have a lower ELF value where delocalisation of electrons is possible.

A LOL is also analyzed to study localized electrons, and the nature of bonds depends on the kinetic energy density [46]. It describes the localized orbital overlaps and the molecule bonding regarding electron density. The LOL ranges from 0 to 0.8. LOL, a value below 0.5 signifies the region of delocalized electron. Figures SF1 a and b show the LOL diagram of the DAHA molecule. Similar to ELF, the localization of electrons is more in the region indicated in red, mainly hydrogen atom-surrounded areas, and the delocalization of electrons is more in blue-shaded regions around carbon and nitrogen in the LOL diagram.

Reactivity descriptors analysis

Molecular electrostatic potential analysis

MEP gives a three-dimensional representation of the dispersion of molecular charge, aiding in comprehending molecular interaction and bond structure. It is also defined as an electric potential or voltage felt by a positive test charge at various points in a molecule. The differently charged regions of molecules are depicted on the map with different colors. In addition to displaying

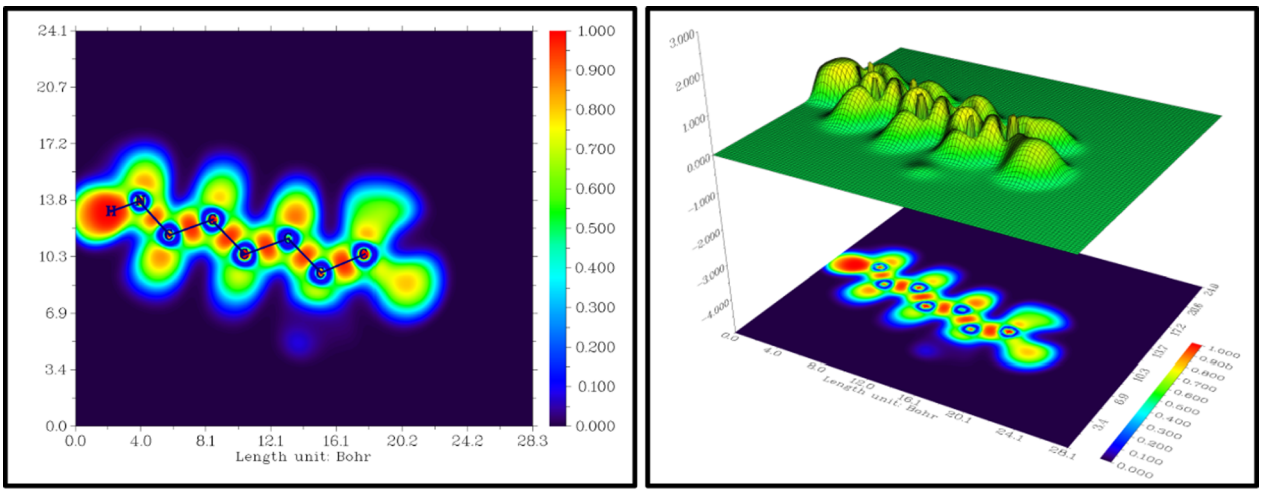

Fig. 5 ELF (**a**) Colour-filled map (**b**) Shaded surface map with projection of DAHA

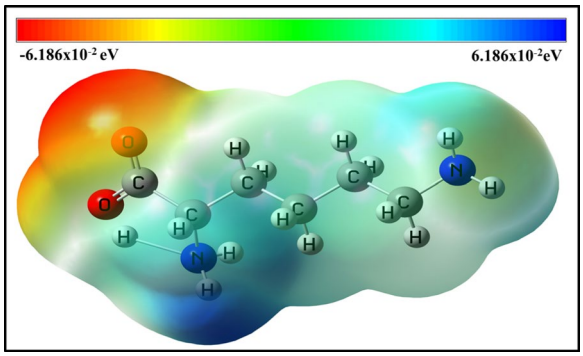

Fig. 6 Molecular electrostatic potential (MEP) diagram of DAHA

charges, these color gradients visualize the shape and size of the molecule. Hence, in organic chemistry, these MEP maps are essential in determining the behavior of complex molecules [47–49]. Figure 6 shows the MEP diagram of the DAHA molecule. The color gradient in the map illustrates the electron density distribution at different regions of the DAHA. The red color indicates the region with a more negative charge, where an electrophilic attack (most substantial repulsion) is more possible, and the blue color indicates the more positively charged region (most potent attraction) while there is a nucleophilic attack. In the electrostatic potential map of DAHA, more red appears in the region where the COOH group is attached, indicating higher electron density around the O3 and O4 atoms of the molecule. Conversely, a more blue color surrounds the hydrogen atoms of the NH3 molecule. H11 and H12 atoms attached to the N7 have a more positive charge in the molecule, that is, less electron density is observed in this region. DAHA molecules have an electrostatic potential range of -6.18×10^{-2} (red) to $+6.18\times10^{-2}$ (blue) in eV. The green color lies between the blue and red range, predominantly representing the neutral areas of the molecule. The color gradient from blue to red indicates the dipole moment direction. In addition to the MEP, other reactivity descriptors such as electronegativity, chemical hardness, and electrophilicity index. These properties were calculated at the molecule's lowest energy geometry, ensuring that the descriptors reflect the most stable configuration of DAHA. This allows for a more accurate prediction of the molecule's reactivity and interaction potential. The MEP diagram was created using the software Gauss View 5.0. It gives a better understanding of the various reaction sites of molecules and their structural character.

Population analysis

The atomic charges of a molecule are significant in calculating various properties. The nuclear charge distribution in the molecule can be analyzed through Mulliken charge distribution [50]. Table ST2 illustrates atomic charges in the DAHA molecule, indicating whether each atom carries a positive or negative charge. These atomic charges, along with other reactivity descriptors such as the Fukui function, electronegativity, chemical hardness, and electrophilicity index, were analyzed together to gain a comprehensive understanding of the molecule's reactivity. By including a range of reactivity descriptors, it can better predict the molecule's potential for interacting with other compounds, which is essential for drug design and molecular engineering. The Mulliken charges of the DAHA molecule range from − 0.45 to 0.45. The color-mapped Figure SF2, also with charge, is given. Red denotes more negative charge, and green indicates more positive charge. Table ST2 shows that atoms C1, C2, O3, O4, C5, N7, C14, C17, and N22 have negative charges, and other atoms possess positive charges. The more negative charge is for the C17 atom, about − 0.45, where the NH_3 group is attached. As amine is an electron-donating group, a considerable increase in the negative charge on the neighboring C17 atom occurs. The most positive charge is for the H13 atom, 0.295 a.u, which is attached to the resonating carboxyl COO– group. Also, the N7 nitrogen atom forms an intramolecular hydrogen bond with the H13 atom. All the localized H-atoms of the DAHA have positive charges. Delocalized lone pair electrons cause a slight negative charge on the carboxyl COO– group.

The Fukui function characterizes the variation in the density of electrons in the frontier molecular orbital due to slight variations in the total electrons [51, 52]. It is important in determining the electrophilic and nucleophilic behavior of a system. The Fukui function uses density functional theory to detect the DAHA's greatest nucleophilic and electrophilic centers. Table 5 and Fig. 7 summarize the Mulliken charges at different bond orbital's, their Fukui functions, and the corresponding local

Table 4 Calculated energy values of DAHA by B3LYP /6-311++G(d, p)

Parameters	Value (eV)
E(HOMO)	− 5.346
E(LUMO)	− 1.756
Ionization potential	− 5.346
Electron affinity	1.756
Energy gap	− 3.590
Electronegativity	− 3.101
Chemical potential	3.101
Chemical hardness	− 2.449
Chemical softness	− 0.408
Electrophilicity index	− 1.963

Table 5 Mulliken charge distribution, Fukui function, and local softness corresponding to (0,1), (-1,2), and (1,2) charge and multiplicity of DAHA

Atom	Mulliken atomic charges			Fukui functions				Local softness		
	N	N − 1	N + 1	fr_+	fr_-	Δf	fr_o	Sr_+fr_+	Sr_-fr_-	Sr_ofr_o
C1	− 0.131	−0.123	0.032	0.163	−0.008	0.171	0.078	−0.091	0.005	−0.044
C2	−0.266	−0.280	1.549	1.815	0.014	1.801	0.915	−1.011	−0.008	−0.510
O3	−0.269	−0.093	−0.311	−0.042	−0.176	0.134	−0.109	0.023	0.098	0.061
O4	−0.168	−0.095	−0.196	−0.028	−0.073	0.045	−0.051	0.016	0.041	0.028
C5	−0.352	−0.372	−0.162	0.19	0.02	0.17	0.105	−0.105	−0.011	−0.058
N7	−0.386	−0.305	−0.378	0.008	−0.081	0.089	−0.037	−0.004	0.045	0.021
C8	0.080	0.079	0.452	0.372	0.001	0.371	0.187	−0.207	−0.001	−0.104
C14	−0.361	−0.382	−1.294	−0.933	0.021	−0.954	−0.456	0.520	−0.012	0.254
C17	−0.450	−0.498	0.887	1.337	0.048	1.289	0.693	−0.745	−0.027	−0.386
N22	−0.331	−0.130	−0.522	−0.191	−0.201	0.01	−0.196	0.106	0.112	0.109

softness. The negative value of function denotes the molecule's gaining of electrons. The electron addition and subtraction to the molecule changes the whole electron system, producing changes in the density of electrons at different sites. Fukui function scrutiny is based on the electron density (ρ(r)) and number of electrons ($N_{electron}$), as it implies that

$$F(r) = \rho(r)/N_{electron}\,.$$

From Table 5, it is clear that there are two types of Fukui functions, $f^+(r)$ and $f^-(r)$. $f^+(r)$ indicates the electron addition to a system ($f^+(r) = \rho_{N+1}(r) - \rho_N(r)$), which represents the nucleophilic reaction, and the $f^-(r)$ indicates the electron removal to a system ($f^+(r) = \rho_N(r) - \rho_{N-1}(r)$) which signifies the electrophilic reaction [53].

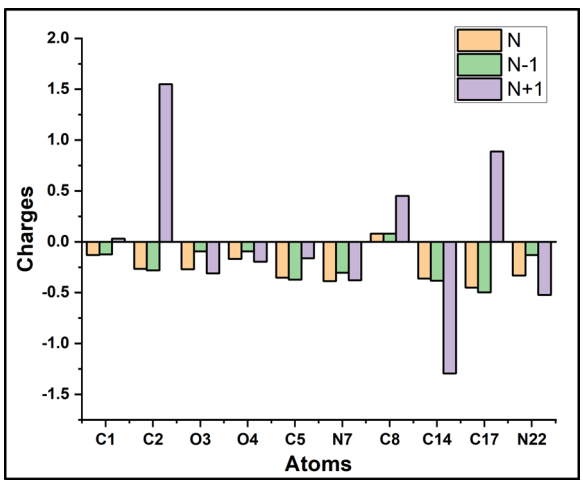

Fig. 7 Graph showing Mulliken atomic charges of DAHA

The reactions occur at the sites with large values of both functions. The atoms with Δf > 0 are the spots for nucleophilic attack, and the table predicts the order C2 > C17 > C8 > C1 > C5 > O3 > N7 > O4 > N22. The atom C14 has a negative value of Δf (− 0.954), a possible site for electrophilic attack. Fukui function analysis determines the local softness, which is significant in biological studies, ligand docking, drug discovery, and protein folding [54]. These reactivity descriptors, calculated using the molecule's most stable geometry, provide insights into DAHA's potential reactivity and suitability as a candidate for further drug development studies.

Thermodynamic properties

Thermodynamic properties of the DAHA were determined at various temperatures using the Atomistica Thermo Online tool, as shown in Table ST3. The temperature increase causes an increase in molecules' vibrational, rotational, and electronic energies. These molecular energy variations result in changes in the Internal energy, Entropy, Enthalpy, Gibbs free energy, and Heat capacities [55, 56].

At 100 K, the values of entropy (S) and heat capacities at constant volume (Cv) and steady pressure (Cp) are 75.358, 20.293, and 22.280 kJ/mol, respectively, which increase to 196.695, 98.987, and 100.974 kJ/mol, respectively, when the temperature rises to 1000 K. From Figure SF3a, it is clear that there is a study increase in the S, Cv, and C_p with an increase in temperature. At 100 K, the values of internal energy (U), enthalpy (H), and Gibbs free energy (G) are − 496.98, − 496.98, and − 496.99 cal/mol K, respectively, and at 1000 K, they become -496.89, -496.89, and -497.19 cal/mol K, respectively. U and H increase with temperature, but G decreases with temperature. This is clear from the Figure SF3b. The values

of thermodynamic properties imply the thermodynamic stability of the DAHA. The thermodynamic properties and temperature dependence are deduced using quadratic regression calculations. A quadratic regression method calculates the correlation coefficient R^2 for thermodynamic properties. The R^2 values for internal energy, enthalpy, Gibbs free energy, and entropy are 0.9998, 0.9998, 0.9999, and 0.9999, respectively. The quadratic regression equation calculated are

$$G = -0.00000007T2 - 0.0001189T - 496.9781667,$$

$$H = 0.0007531T2 - 1.2499577T - 0.0043333,$$

$$S = -0.0000423T2 + 0.1797151T + 58.8885,$$

$$U = 0.0014296T2 - 1.8000679T - 23.4102414,$$

$$Cp = -0.0000523T2 + 0.1468731T + 6.6821667,$$

$$Cv = -0.0000523T2 + 0.1468731T + 6.6821667.$$

The thermodynamic properties determine the conditions required for a chemical reaction. Furthermore, thermodynamic properties define the bonding interaction mode through non-covalent interactions, including hydrophobic effects, hydrogen bonds, electrostatic contacts, and van der Waals interactions. They also give the progress of a reaction and its stability [57]. Figure SF4 (a, b, c, d, e, and f) displays plots of equations.

Reduced density gradient (RDG)

RDG analysis studied the various non-covalent contacts in molecules based on the reduced density gradient. It helps to examine intra- and inter-non-bonded interactions within a molecule [58]. RDG is based on electron density, highlighting the low electron density regions. These regions indicate the non-covalent interaction [59, 60].

The gradient iso-surfaces and scatter graphs of the DAHA are shown in Fig. 8. Figures were plotted using the Multiwfn programme. The scatter graph is RDG versus sign(λ2)ρ plot. The greatest eigenvalue of the matrix of Hessian is denoted as λ2, where sign(λ2)ρ is the second eigenvalue of electron density. The value and sign of sign(λ2)ρ provide information on the nature of interaction [61]. RDG ranges between -0.035 a.u and 0.020 a.u. Positive and negative sign values (λ2)ρ specify the repulsive and attractive interaction, respectively, whereas nearly zero value is for weak interactions. Scatter spectra are splits into red, green and blue colours. The red spikes of RDG isosurface show the repulsion due to steric hindrance observed in the molecule, mainly by the carboxyl group. From the scatter graph, the red form ranges between 0.02 a.u and 0.04 a.u, showing the strong repulsive contribution. The blue spikes manifest the strong attraction due to the H-bonding of the Amino group, N–H…O. Its contour ranges from − 0.04 a.u to − 0.02 a.u, confirming the existence of strong H-bonding. The green areas demonstrate the van der Waals interaction. Consequently, interacting areas in the structure of DAHA are shown using RDG graphs.

Non-linear optical analysis (NLO)

Non-linear optical analysis describes the nonlinear responses of the polarization density to the electric field of light. Insulating crystals form second-order NLO materials. A non-centrosymmetric molecule usually shows non-linear behavior when it interacts with electromagnetic radiation. Dipole moments of the materials are proportional to the higher powers of the field intensity. NLO properties are related to polarizabilities and hyperpolarizabilities. Hence, for a nonlinear response, hyperpolarizability is always nonzero [62–64]. Highly polarizable molecules possess strong NLO potential, with organic compounds being the primary focus for NLO materials due to their more efficient response than inorganic ones. Those materials with lower HOMO–LUMO energy gaps show better NLO properties. The substituents, molecular configuration, pi-conjugation system length, and type of compound are responsible for the NLO properties. The non-linear optical materials are used in various optoelectronics and other optical devices [65–67].

DAHA, an organic molecule containing heteroatoms, exhibits promising NLO properties, as explored in the NLO analysis. To analyse the dipole moment (μ), static polarizability (α_0), and first-order hyperpolarizability (β) of the DAHA molecule, the Polarization properties were estimated computationally using B3LYP/6-3++G (d, p) function within DFT technique. The given Table 6 shows the dipole moment (μ_X μ_Y μ_Z) polarizability (α_{XX} α_{XY} α_{YY} α_{XZ} $\alpha_{YZ\ and}$ α_{ZZ}) and hyperpolarizability (β_{XXX} β_{YYY} β_{ZZZ} β_{XYY} β_{XXY} β_{XXZ} β_{XZZ} β_{YZZ} $\beta_{YYZ\ and}$ β_{XYZ}) coefficients obtained from the Gaussian frequency output file. For a better understanding of NLO responses, dipole polarizabilities are essential. The average polarizability or static polarizability (α_o) exhibits three major components ($\alpha_{XX,}$ $\alpha_{YY,}$ and α_{ZZ}), and the First-order hyperpolarizability or static second-order polarizability (β) has ten components. The equation for the calculation of α_o and $_\beta$ are given:

$$\alpha_0 = (\alpha_{XX} + \alpha_{YY} + \alpha_{ZZ}),$$

$$\beta_{tot} = [(\beta_{XXX} + \beta_{XYY} + \beta_{XZZ})^2 + (\beta_{YYY} + \beta_{XXY} + \beta_{YZZ})^2 + (\beta_{ZZZ} + \beta_{XXZ} + \beta_{YYZ})^2],$$

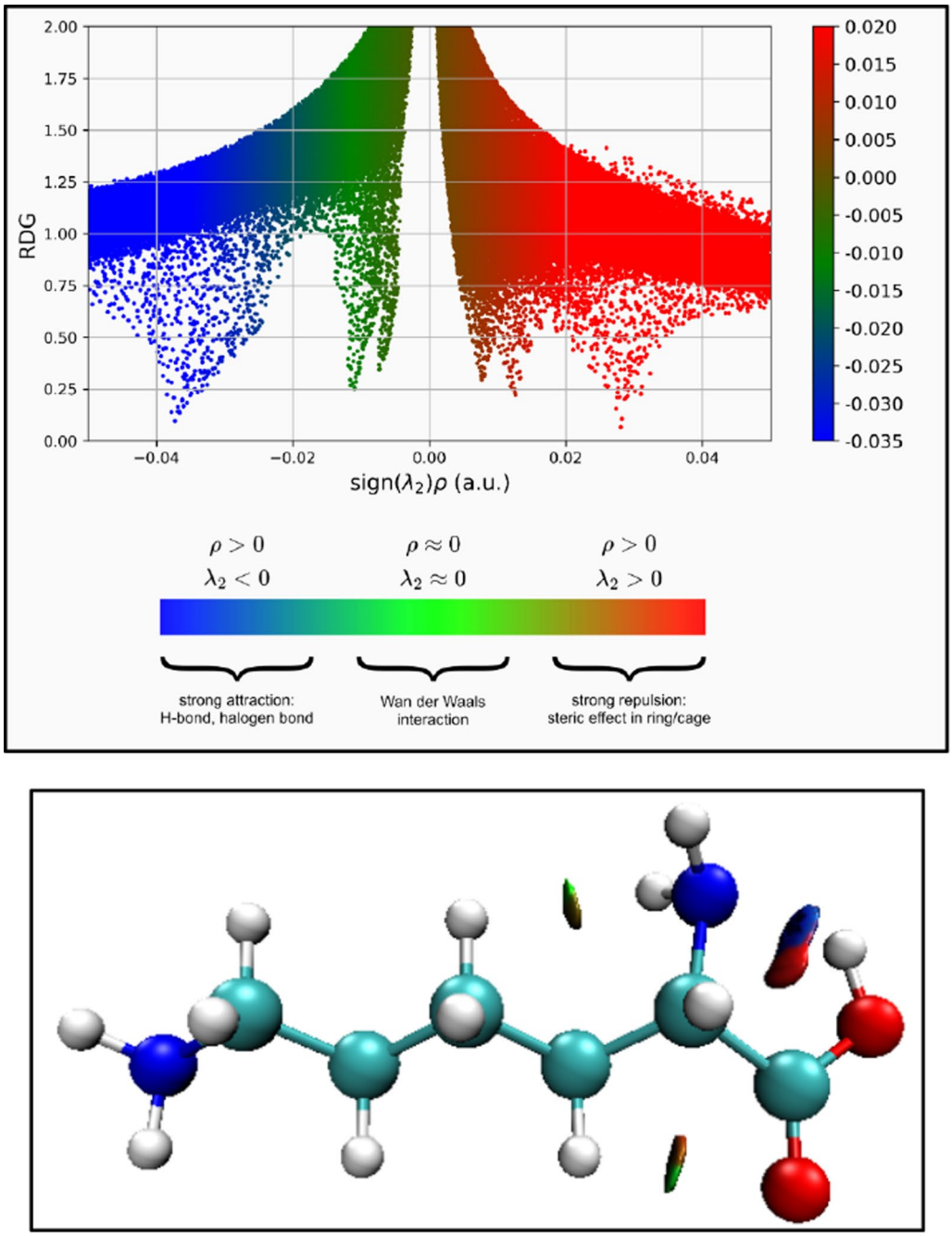

Fig. 8 2D and 3D isosurface of DAHA generated using the 6-311++G(d,p) basis set

To compare the DAHA's NLO values, the Urea's NLO threshold values were studied using DFT with function B3LYP and -311++G (d, p) basis set [68, 69]. The molecules' total static dipole moment is 12.2549 D. A Higher dipole moment reflects a high degree of intermolecular interaction. The more significant contribution of dipole moment is along the X direction. The static polarizability (α_0) of DAHA − 10.87×10^{-24} esu was less compared with urea 0.9771×10^{-23}. The First-order hyperpolarizability (β) was 1.752×10^{-30} esu for DAHA, it is more than that of urea 0.927×10^{-30}. β_{XXX} shows the largest value, mainly contributing to the hyperpolarizability and charge transfer, which is major along the x direction. The computed α and β units are in atomic units. It is converted to esu as (α:1 a.u. = 0.1482×10^{-24} esu, β: 1a.u. = 8.6393×10^{-33} esu). The values of polarizability

Table 6 The calculated dipole moment μ(D), polarizability (α_0), first-order hyperpolarizability, (β_{tot}) values of the DAHA molecule

Parameters	B3LYP/6-311++G(d,p)	Urea	Parameters	B3LYP/6-311++G(d,p)	Urea
μ_X	8.7347	−0.806	β_{XXX}	164.5451	23.748
μ_Y	8.0445	1.543	β_{YYY}	35.1255	44.220
μ_Z	−3.0290	−0.008	β_{ZZZ}	−5.9980	−1.062
μ(D)	12.2549	−1.741	β_{XYY}	3.9851	−55.468
α_{XX}	−98.1134	37.245	β_{XXY}	53.2645	17.376
α_{XY}	−20.5323	−0.194	β_{XXZ}	−53.6373	−0.489
α_{YY}	−53.9168	37.988	β_{XZZ}	0.6682	−19.037
α_{XZ}	−1.0862	0.052	β_{YZZ}	7.4760	33.038
α_{YZ}	−2.8356	−0.063	β_{YYZ}	2.1061	−0.531
α_{ZZ}	−68.0395	24.012	β_{XYZ}	15.3534	0.034
α_0(e.s.u)	-10.87×10^{-24}	0.9771×10^{-23}	β_{tot} (e.s.u)	1.752×10^{-30}	0.927×10^{-30}

and hyperpolarizability are considered for further NLO analysis.

Biological assessment

Drug likeness

Drug likeness is a concept that assesses whether a specific compound possesses the essential properties to be a feasible medication for therapeutic applications. It consists of a set of properties that indicate the propensity of a chemical compound to be considered a drug candidate. Its main goal is to find the molecules with a better chance of being absorbed, distributed, metabolized, and eliminated (ADME) safely and effectively treating a particular disease. Some rules exist to determine drug-likeness based on a specific compound's structural, physicochemical, and pharmacokinetic properties. Lipinski's rule of five consists of some standards of medicinal chemistry and drug analysis to evaluate the drug-likeness of small organic molecules. Other rules like Veber's, Ghose's, MDDR, BBB, and CMC 50 are extensions of Lipinski's rule [70, 71].

Drug likeness analysis was implemented on the DAHA and its derivatives. The SMILES notation of the DAHA molecule was obtained from PubChem, and the Swiss ADME site was utilized for the analysis. Table 7 provides the analyzed results. According to Lipinski's rule, for higher chances of becoming a successful oral drug, the H-bond donor (HBD) and H-bond acceptor (HBA) should possess a value less than or equal to 5 and 10, respectively [72]. Molar refractivity should be between 40–130, and Topology polar surface area (TPSA) should be less than 140 $Å^2$. From Table 7, it's clear that the values of HBD, HBA, MR, and TPSA of the DAHA molecule and its derivative fall under these ranges. The TPSA values of all compounds come under a range between 85.16 and 126.64, and Molar refractivity is related to the size and flexibility of a molecule, which can influence its ability to interact with biological targets. A compound with an optimal molar refractivity value is likely to have favorable pharmacokinetic properties, such as absorption and distribution, contributing to its overall efficacy as a drug candidate. In the context of DAHA, the MR values fall within a range of 38.14 to 55.98 cm^3/mol, suggesting that these compounds possess suitable molecular characteristics for potential drug development. The bioavailability of DAHA and its derivatives is 0.55. GI (Gastrointestinal), Bioavailability, BBB (blood–brain barrier), and CYP1A2 are the drug-likeness properties related to absorption, distribution, and metabolism. All the compounds have high GI absorption and no BBB permeant.

Table 7 ADME properties of DAHA

Derivative	HBD	HBA	MR	TPSA A^2	GI absorption	BBB permaent	CYP1A2 inhibitor	LogKp (cm/s)	Lipinski violations	Bioavailability score
DAHA	3	4	38.14	89.34	High	No	No	− 9.36	Yes	0.55
L-lysine acetate	4	6	51.64	126.64	High	No	No	− 11.49	Yes	0.55
L-lysine hydrochloride	3	4	45.11	89.34	High	No	No	− 9.01	Yes	0.55
L-Lysinamide	3	3	39.28	95.13	High	No	No	− 8.19	Yes	O.55
L-lysine diisocyanate	0	6	55.98	85.16	High	No	No	− 5.32	Yes	0.55

The DAHA and its derivatives follow Lipinski's rule of five and exhibit anti-herpes simplex viral and anti-osteoporotic activity [73, 74]. The compounds' high gastrointestinal absorption and favorable pharmacokinetic properties (as indicated by the drug-likeness analysis) support their potential as oral therapeutics for osteoporosis.

Molecular docking

Molecular docking is a computational technique that is of great importance in the field of drug discovery. It is a technique to predict an optimized conformation and preferred orientation of ligands and receptors to form a stable complex. The ligand-receptor complex conformation with minimum free energy is preferred for pharmaceutical purposes. It predicts the binding affinity, the binding site's geometry, and the drug's design [75–77]. Molecular docking is conducted using the software Autodock Vina. Chimera 1.17.3 is used for the molecular docking of DAHA molecules to visualize the 3D structure and their interaction and analyze the complex structure's binding site and binding energy. The protein ID of the target is taken from the SwissADME-Target prediction site and downloaded from PDB (Protein data bank). Using Chimera 1.17.3, The downloaded proteins were optimized and cleaned by eliminating more residues and water molecules [78, 79]. The 3CHO, 3U9W, 5N12, 4MKT, and 2XMB are some hydrolase proteins that were docked with the DAHA molecule, and the H-bond distance between the DAHA and the targets (3CHO, 3U9W, 5N12, 4MKT, and 2XMB) were depicted in Fig. 9a and

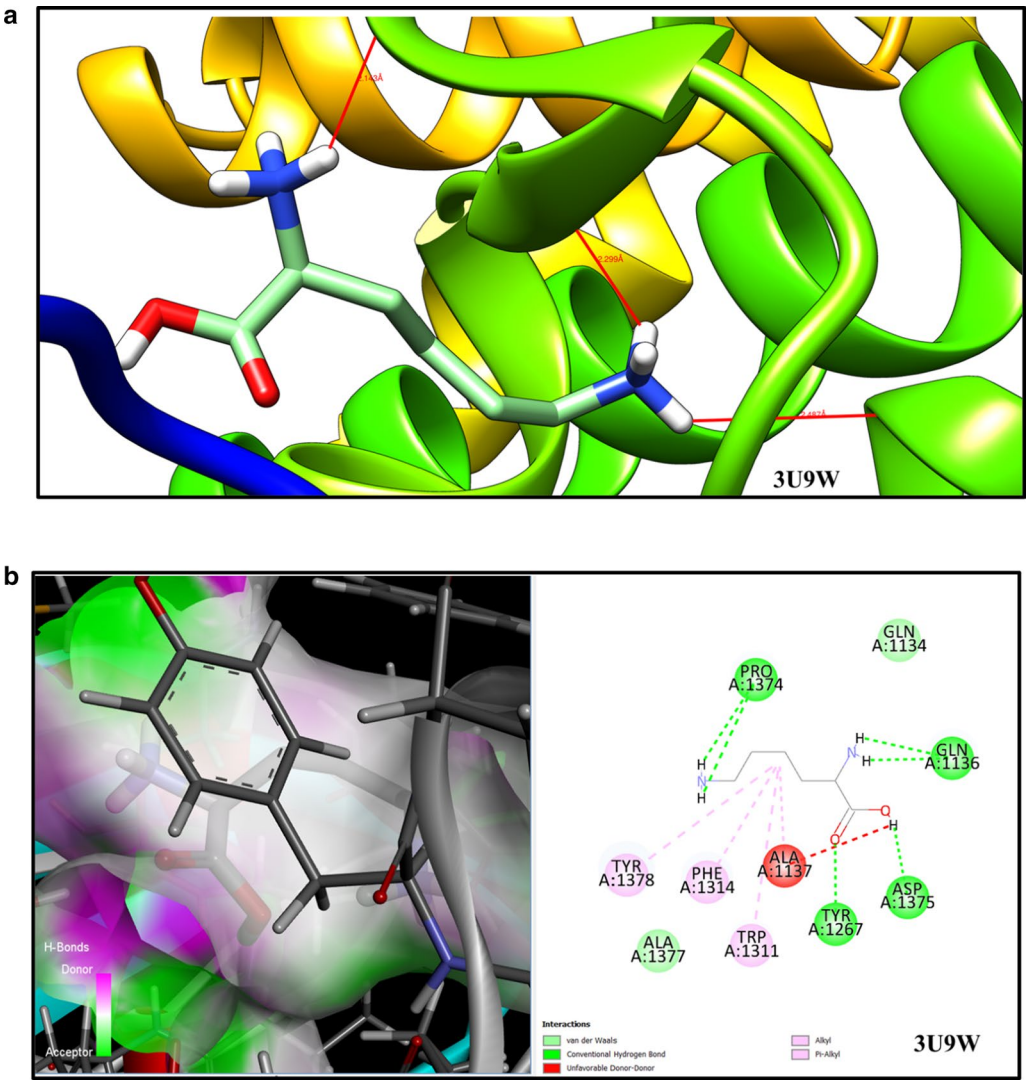

Fig. 9 **a** DAHA embedded in the active site of 3U9W protein, **b** 2D molecular docking of DAHA

SF5. The docking parameters (bond distance, binding energy, and RMSD reference) were analyzed in Table 8. The 3CHO, 3U9W, and 5N12 have the highest binding energy of − 0.5 kcal/mol. And the least binding energy for 2XMB at − 4.6 kcal/mol. All the proteins have three residues with a hydrogen bonding ranging from 1.9 to 2.5 (E). The choice of hydrolase enzymes as target proteins for DAHA docking studies was based on their involvement in key metabolic processes that DAHA could potentially influence. Hydrolases play significant roles in the breakdown and synthesis of biomolecules, including proteins, lipids, and carbohydrates, which are crucial for various physiological functions. The selection of hydrolases aims to explore how DAHA interacts with enzymes involved in key metabolic pathways, such as protein degradation, energy metabolism, and neurotransmitter synthesis, thereby deepening the understanding of its potential therapeutic applications.

The 2D analysis of molecular docking of DAHA is done using the Discovery Studio tool, as shown in Fig. 9b and SF5. It gives a clear-cut picture of the ligand's interaction with each protein's various amino acids and its specific orientation. In each protein receptor, the table Hydrogen of the amino group of the DAHA molecule interacts with amino acids like HIS, GLU, PRO, ALA, ASP, and GLY. The oxygen atom also interacts with the amino acids of receptors like GLY, HIS, SER, and TRY. The Hydrogen atoms attached to the carbon of the titled molecule show some interaction with the amino acids TRY and PHE. The different kinds of interactions are shown in the diagram with various colors. Most of the interactions are through conventional Hydrogen bonding. Like Pi-sigma, alkyl and donor-donor interactions between the Ligand and the receptor are present. This confirms that the interaction between the ligand and protein forms a stable complex structure suitable for drug discovery and other biological effects [80]. The biological significance of DAHA has been elaborated in the manuscript, emphasizing their potential therapeutic applications, particularly in anti-herpes and anti-osteoporotic activities. These findings highlight the potential of DAHA as a drug candidate. This includes investigating their involvement in specific metabolic and signaling pathways and elucidating their mechanisms of action at the molecular and cellular levels. Such studies would provide valuable insights into the therapeutic potential of these molecules and pave the way for the development of more targeted and effective drugs.

Table 8 Hydrogen bonding and molecular docking with Centromere-associated protein inhibitor protein targets

Protein (PDB ID)	No of Residues	Bond distance (Å)	Binding energy (kcal/mol)	Reference RMSD (Å)
3CHO	3	1.991, 2.123	− 5.5	6.641
3U9W	3	2.143, 2.487, 2.299	− 5.5	2.05
5NI2	3	2.180	− 5.5	2.82
4MKT	3	2.345	− 5.3	2.162
2XMB	3	2.422, 2.106	− 4.6	5.561

Conclusion

This research summarizes the theoretical and experimental analysis of the DAHA molecule. The given compound investigated quantum chemically using Density Functional Theory (DFT) by B3LYP method with the 6-311G++(d,p), and other calculations were done using different software. The molecule was described experimentally through FT-IR and UV analysis. The computationally conducted molecular structure and optical studies were compared to experimental data with positive findings were observed when comparing the computed data of the DAHA with experimental data. The optimization of DAHA was done, and it was found to be a molecule with singlet spin and a C1 point group with a dipole moment of 5.8381 Debye. The vibrational analysis was conducted by examining the FT-IR spectra with a PED assignment using the VEDA program. The stretching, bending, and torsional vibrations of groups like NH2, COOH, CH, CH2, CC, and CN were studied separately. The UV spectra of the DAHA were determined experimentally in methanol as solvent and estimated theoretically in gaseous form, DMSO, and methanol. The absorption peak does not change significantly when exposed to different solvents and agrees with the investigational values. The FMO analysis with different HOMO–LUMO transitions examined the reactivity and stability of DAHA, with a bandgap energy of − 3.591 eV, highlighting the molecule's stability. The ELF and MEP analysis was carried out, and various color codes were used to study the reactivity and stability. DAHA molecules have an electrostatic potential range of -6.18×10^{-2} (red) to $+6.18\times10^{-2}$ (blue). Mulliken analysis and Fukui population studies were examined to determine each atom's atomic charges and other electrophilic and nucleophilic characteristics. In given compound, the electrophilic site is C14 and the nucleophilic reactivity order C2 > C17 > C8 > C1 > C5 > O3 > N7 > O4 > N22. Greater stabilization in DAHA molecule as affirmed by the delocalization of electron of σ (O4–H13) to σ* (C1–O3) of 6.09 kcal/mol and followed by σ (C5–H10) to σ* (C2–N7) of 4.88 kcal/mol and σ (C2–H6) to σ* (C1–O3) of 4.09 kcal/mol. The temperature dependence on various properties was calculated and plotted using

the Atomistica thermo online program. The molecule is an organic molecule with hetero atoms and good NLO properties. The titled molecule did not show non-linear optical properties compared to the reference compound urea. According to the drug-likeness, the molecule and its derivatives follow Lipinski's rule of five, showing anti-herpes simplex viral and anti-osteoporotic activity. The medical use of the molecule was found using its protein–ligand approach, and the resulting binding energy is − 5.5 kcal/mol when it is attached to the proteins 3CHO, 3U9W, and 5N12 suggesting its suitability for further pharmaceutical applications. This article comprehensively analyzes the DAHA molecule's geometry, spectrometry, electronic state, and biological importance, providing valuable insights into its potential applications in various fields.

Supplementary Information

The online version contains supplementary material available at https://doi.org/10.1186/s13065-025-01511-4.

Supplementary Material 1.

Acknowledgements
We acknowledgement Jamia Millia Islamia, New Delhi and Dayalbagh Educational Institute, Agra, for facility and infrastructure.

Author contributions
Amna Sherin T: Writing—original draft, Abdul Nazar P. V: Writing—original draft, Sandhya Savita: Analysis, visualization, Mudassar Shahid: Data curation, Analysis, Nazia Siddiqui: Writing—review and editing. Saleem Javed: Conceptualization, Software, Supervision.

Funding
This research was supported by Researchers Supporting Project number (RSPD2025R1005), King Saud University, Riyadh, Saudi Arabia.

Availability of data and materials
All the data used present in the manuscript or supplementary material.

Declarations

Ethics approval and consent to participate
Not applicable as our research doesn't involve humans or animals.

Consent for publication
Not applicable.

Competing interests
The authors declare no competing interests.

Received: 2 November 2024 Accepted: 13 May 2025
Published online: 29 May 2025

References

1. Hayamizu K, Oshima I, Fukuda Z, Kuramochi Y, Nagai Y, Izumo N, Nakano M. Safety assessment of L-lysine oral intake: a systematic review. Amino Acids. 2019;51:647–59. https://doi.org/10.1007/s00726-019-02697-3.
2. Pedrazini MC, da Silva MH, Groppo FC. L-lysine: its antagonism with L-arginine in controlling viral infection. Narrative literature review. Br J Clin Pharmacol. 2022;88:4708–23. https://doi.org/10.1111/bcp.15444.
3. Shankar K, Sakthibalan M, Raizada P, Jain R. A randomized open-label clinical study comparing the efficacy, safety, and bioavailability of calcium lysinate with calcium carbonate and calcium citrate malate in osteopenia patients. J Orthopaedic Case Rep. 2018;8:15. https://doi.org/10.13107/jocr.2250-0685.1138.
4. Shashikumara S, Jayaraman V, Chikkegowda P, Channapatna Lingaiah D, Sukhlal Kalal B. Efficacy of 15% lysine cream in treating diabetic foot ulcers: a randomised interventional study. Int J Physiol Pathophysiol Pharmacol. 2023;15:88.
5. Hong Y, Najafi S, Casey T, Shea JE, Han SI, Hwang DS. Hydrophobicity of arginine leads to reentrant liquid–liquid phase separation behaviors of arginine-rich proteins. Nat Commun. 2022;13:7326. https://doi.org/10.1038/s41467-022-35001-1.
6. An S, Ahn S, Letona A, Shin JH, Kang SH, Jeong JY, Park SM, Kim JW, Yu D, Chung H, Chung D. Moisture sorption, thermal, and caking characteristics of L-lysine-carbonate granules. Food Biosci. 2023;53: 102845. https://doi.org/10.1016/j.fbio.2023.102845.
7. Eggeling L, Bott M. A giant market and a powerful metabolism: L-lysine provided by Corynebacterium glutamicum. Appl Microbiol Biotechnol. 2015;99:3387–94. https://doi.org/10.1007/s00253-015-6508-2.
8. Kloss R, Limberg MH, Mackfeld U, Hahn D, Grünberger A, Jäger VD, Krauss U, Oldiges M, Pohl M. Catalytically active inclusion bodies of L-lysine decarboxylase from E. coli for 1,5-diaminopentane production. Sci Rep. 2018;8:5856. https://doi.org/10.1038/s41598-018-24070-2.
9. Mailoo VJ, Rampes S. Lysine for herpes simplex prophylaxis: a review of the evidence. Integr Med Clin J. 2017;16:42.
10. Li M, Shen X, Liu M, Lu J. Synthesis TS-1 nano zeolites via L-lysine assisted route for hydroxylation of benzene. Mol Catal. 2021;513: 111779. https://doi.org/10.1016/j.mcat.2021.111779.
11. Chen S, Huang S, Li Y, Zhou C. Recent advances in epsilon-poly-L-lysine and L-lysine-based dendrimer synthesis, modification, and biomedical applications. Front Chem. 2021;9: 659304. https://doi.org/10.3389/fchem.2021.659304.
12. Wendisch VF. L-lysine. In: Industrial biotechnology: products and processes. New York: Wiley; 2017. p. 361–90. https://doi.org/10.1002/9783527807833.ch12.
13. Savita S, Fatima A, Bhattacharya P, Saral A, Haq N, Muthu S, Sahu BL, Siddiqui N, Javed S. Spectroscopic, quantum computational, molecular dynamic simulations, and molecular docking investigation of the biologically important compound-2,6-diaminopyridine. Spectrosc Lett. 2024;58:195–213. https://doi.org/10.1080/00387010.2024.2424453.
14. Pathan HK, Fatima A, Garg P, Muthu S, Yadav A, Siddiqui N, Ali M, Javed S. Spectroscopic, computational, molecular docking and dynamics simulations studies of 4-amino-3-hydroxyNaphthalene-1-sulfonic acid (ANSA). Polycycl Aromat Compd. 2024;44(6):3787–806. https://doi.org/10.1080/10406638.2023.2239981.
15. Savita S, Jeba Reeda VS, Siddiqui N, Arora H, Khilari S, Shahid M, Sahu BL, Javed S. Molecular insights into 5-hydroxymethylfurfural: a computational, spectroscopic, and docking investigation. Spectrosc Lett. 2024;58:113. https://doi.org/10.1080/00387010.2024.2410816.
16. Ahmad S, Reeda VJ, Aziz K, Arora H, Kumar M, Garima K, Ali A, Shahid M, Muthu S, Siddiqui N, Javed S. Multifaceted investigation of sulfamerazine: insights from computational methods, experimental techniques, and molecular simulations. J Mol Struct. 2024;1312: 138554. https://doi.org/10.1016/j.molstruc.2024.138554.
17. Kumari C, Savita S, Reeda VJ, Shahid M, Siddiqui N, Javed S. Unlocking the enigma: spectroscopic insights, molecular modelling, molecular docking, simulation and MMPBSA analysis of L-ornithine. J Mol Liq. 2024;414: 126108. https://doi.org/10.1016/j.molliq.2024.126108.
18. Ahmad S, Kumar M, Garima K, Ali A, Arora H, Muthu S, Javed S. DFT, molecular docking, molecular dynamics simulation, and Hirshfeld surface analysis of 2-phenylthioaniline. Polycycl Aromat Compd. 2024;44(9):5876–98. https://doi.org/10.1080/10406638.2023.2270128.
19. Garima K, Savita S, Mishma JC, Reeda VJ, Muthu S, Siddiqui N, Javed S. Quantum computational, spectroscopic analysis, and molecular docking studies of 2-chloroethyl benzene. Discov Chem. 2024;1(1):54. https://doi.org/10.1007/s44371-024-00061-3.

20. Reeda VJ, Divya P, Ranchani AAJ, Manikandan A, Alvi S, Ali R, Siddiqui N, Haq N, Muthu S, Butcher R, Javed S. Comprehensive analysis of 2,5-dimethyl-1-(naphthalen-1-yl)-1*H*-pyrrole: X-ray crystal structure, spectral, computational, molecular properties, docking studies, molecular dynamics, and MMPBSA. J Mol Struct. 2025;1321: 140062. https://doi.org/10.1016/j.molstruc.2024.140062.
21. Frisch MJ, Trucks GW, Schlegel HB, Scuseria GE, Robb MA, Cheeseman JR, Scalmani G, Barone V, Mennucci B, Petersson G, Nakatsuji H. Gaussian 09. Wallingford: Gaussian Inc.; 2009.
22. Petersson A, Bennett A, Tensfeldt TG, Al-Laham MA, Shirley WA, Mantzaris J. A complete basis set model chemistry. I. The total energies of closed-shell atoms and hydrides of the first-row elements. J Chem Phys. 1988;89:2193–218. https://doi.org/10.1063/1.455064.
23. Petersson GA, Al-Laham MA. A complete basis set model chemistry. II. Open-shell systems and the total energies of the first-row atoms. J Chem Phys. 1991;94:6081–90. https://doi.org/10.1063/1.460447.
24. Jamroz MH. Vibrational energy distribution analysis (VEDA): scopes and limitations. Spectrochim Acta Part A Mol Biomol Spectrosc. 2013;114:220–30. https://doi.org/10.1016/j.saa.2013.05.096.
25. Alecu IM, Zheng J, Zhao Y, Truhlar DG. Computational thermochemistry: scale factor databases and scale factors for vibrational frequencies obtained from electronic model chemistries. J Chem Theory Comput. 2010;6(9):2872–87. https://doi.org/10.1021/ct100326h.
26. Lu T, Chen F. Multiwfn: a multifunctional wavefunction analyzer. J Comput Chem. 2012;33:580–92. https://doi.org/10.1002/jcc.22885.
27. Orji EI, Ugwu AC, Ugwuanyi CM, Cyril M, Uwakwe EC, Elejere UC, Omeke NE, Ugwuanyi CS. Reducing errors in slope in physics graphs using origin lab software. Webology 2022;19(3).
28. Daina A, Michielin O, Zoete V. Swiss ADME: a free web tool to evaluate pharmacokinetics, druglikeness and medicinal chemistry friendliness of small molecules. Sci Rep. 2017;7:42717. https://doi.org/10.1038/srep42717.
29. Butt SS, Badshah Y, Shabbir M, Rafiq M. Molecular docking using Chimera and AutoDock Vina software for nonbioinformaticians. JMIR Bioinf Biotechnol. 2020;1:14232. https://doi.org/10.2196/14232.
30. Welden AR, Phillips JJ, Zgid D. Ionization potentials and electron affinities from the extended Koopmans' theorem in self-consistent Green's function theory. arXiv preprint arXiv:1505.05575, 2015. https://doi.org/10.48550/arXiv.1505.05575.
31. Low JN, Glidewell C. A quasi-diamondoid hydrogen-bonded framework in anhydrous sulfanilic acid. Acta Crystallogr C. 2002;58:o209–11. https://doi.org/10.1107/S0108270102003025.
32. Savita S, Fatima A, Garima K, Pooja K, Verma I, Siddiqui N, Javed S. Experimental spectroscopic, Quantum computational, Hirshfeld surface and molecular docking studies on 3-Pyridinepropionic acid. J Mol Struct. 2021;1243: 130932. https://doi.org/10.1016/j.molstruc.2021.130932.
33. Issaoui N, Rekik N, Oujia B, Wojcik MJ. Theoretical infrared line shapes of H-bonds within the strong anharmonic coupling theory and Fermi resonances effects. Int J Quantum Chem. 2010;110:2583–602. https://doi.org/10.1002/qua.22395.
34. Temsamani MA, Xu LH, Lees RM. A rotation–torsion–vibration treatment with three-dimensional internal coordinate approach and additional FTIR spectral assignments for the CH3-bending fundamentals of methanol. J Mol Spectrosc. 2003;218:220–34. https://doi.org/10.1016/S0022-2852(02)00087-5.
35. Roeges NP, Baas JMA. A guide to the complete interpretation of infrared spectra of organic structures. New York: Wiley; 1994. p. 122.
36. Fatima A, Pooja K, Savita S, Singh M, Verma I, Siddiqui N, Javed S. Quantum chemical, experimental spectroscopic, Hirshfeld surface and molecular docking studies of the anti-microbial drug Sulfathiazole. J Mol Struct. 2021;1245: 131118. https://doi.org/10.1016/j.molstruc.2021.131118.
37. Shoba D, Periandy S, Boomadevi S, Ramalingam S, Fereyduni E. FT-IR, FT-Raman, UV, NMR spectra, molecular structure, ESP, NBO, and HOMO–LUMO investigation of 2-methylpyridine 1-oxide: a combined experimental and DFT study. Spectrochim Acta Part A Mol Biomol Spectrosc. 2014;118:438–47. https://doi.org/10.1016/j.saa.2013.09.023.
38. Xavier S, Periandy S. Spectroscopic (FT-IR, FT-Raman, UV, and NMR) investigation on 1-phenyl-2-nitropropene by quantum computational calculations. Spectrochim Acta Part A Mol Biomol Spectrosc. 2015;149:216–30. https://doi.org/10.1016/j.saa.2015.04.055.
39. Mhareb MHA, Hashim S, Sharbirin AS, Alajerami YSM, Dawaud RSES, Tamchek N. Physical and optical properties of Li_2O-MgO-B_2O_3 doped with Dy^{3+}. Opt Spectrosc. 2014;117:552–9. https://doi.org/10.1134/S0030400X14100166.
40. Rekik N, Issaoui N, Ghalla H, Oujia B, Wojcik MJ. Infrared spectral density of H-bonds within the strong anharmonic coupling theory: indirect relaxation effect. J Mol Struct. 2007;844:21–31. https://doi.org/10.1016/j.molstruc.2007.02.040.
41. Fatima A, Khanum G, Sharma A, Garima G, Savita S, Verma I, Siddiqui N, Javed S. Computational, spectroscopic, Hirshfeld surface, electronic state and molecular docking studies on phthalic anhydride. J Mol Struct. 2022;1249: 131571. https://doi.org/10.1016/j.molstruc.2021.131571.
42. Roy DR, Parthasarathi R, Maiti B, Subramanian V, Chattaraj PK. Electrophilicity as a possible descriptor for toxicity prediction. Bioorg Med Chem. 2005;13:3405–12. https://doi.org/10.1016/j.bmc.2005.03.011.
43. Fatima A, Singh M, Singh N, Savita S, Verma I, Siddiqui N, Javed S. Investigations on experimental, theoretical spectroscopic, electronic excitations, molecular docking of Sulfaguanidine (SG): an antibiotic drug. Chem Phys Lett. 2021;783: 139049. https://doi.org/10.1016/j.cplett.2021.139049.
44. Becke AD, Edgecombe KE. A simple measure of electron localization in atomic and molecular systems. J Chem Phys. 1990;92(9):5397–403. https://doi.org/10.1063/1.458517.
45. Fatima A, Khanum G, Savita S, Pooja K, Verma I, Siddiqui N, Javed S. Quantum computational, spectroscopic, Hirshfeld surface, electronic state and molecular docking studies on sulfanilic acid: an anti-bacterial drug. J Mol Liq. 2022;346: 117150. https://doi.org/10.1016/j.molliq.2021.117150.
46. Jacobsen H. Localized-orbital locator (LOL) profiles of chemical bonding. Can J Chem. 2008;86:695–702. https://doi.org/10.1139/v08-052.
47. Fradi T, Noureddine O, Taheur FB, Guergueb M, Nasri S, Amiri N, Almahri A, Roisnel T, Guerineau V, Issoui N, Nasri H. New DMAP meso-arylporphyrin magnesium (II) complex. Spectroscopic, cyclic voltammetry and X-ray molecular structure characterization. DFT, DOS and MEP calculations and antioxidant and antifungal activities. J Mol Struct. 2021;1236: 130299. https://doi.org/10.1016/j.molstruc.2021.130299.
48. Cramer CJ, Bickelhaupt FM. Essentials of computational chemistry. Angewandte Chemie Int Edn Engl. 2003;42:381.
49. Manhas FM, Fatima A, Verma I, Siddiqui N, Muthu S, AlSalem HS, Savita S, Singh M, Javed S. Quantum computational, spectroscopic (FT-IR, NMR and UV–Vis) profiling, Hirshfeld surface, molecular docking and dynamics simulation studies on pyridine-2,6-dicarbonyl dichloride. J Mol Struct. 2022;1265: 133374. https://doi.org/10.1016/j.molstruc.2022.133374.
50. Wiberg KB, Rablen PR. Atomic charges. J Org Chem. 2018;83(24):15463–9. https://doi.org/10.1021/acs.joc.8b02740.
51. Sanchez Marquez J. New advances in conceptual-DFT: an alternative way to calculate the Fukui function and dual descriptor. J Mol Model. 2019;25:1–7. https://doi.org/10.1007/s00894-019-4000-0.
52. Dong Y, Xu D, Liao S, Fang X, Chen J, Qu W, Hu X, Ma Z, Zhao J, Gu X, Tang X. Frontier band orbitals of active sites in single-atom catalysis. J Phys Chem C. 2024;128:2884–93. https://doi.org/10.1021/acs.jpcc.3c08006.
53. Gupta S, Savita S, Prakash A, Khan T, Hashmi K, Joshi S. Synthesis, DFT and carbamothioylhydrazineylidene) methyl) benzoic acid. J Mol Struct. 2023;1293: 136276. https://doi.org/10.1016/j.molstruc.2023.136276.
54. Maheswari CU. QM, Fukui function, molecular docking, molecular dynamics investigation on Human Estrogen Receptor (HER) with Clioquinol. Chem Phys Impact. 2024;8: 100570. https://doi.org/10.1016/j.chphi.2024.100570.
55. Armaković S, Armaković SJ. Atomistica. Online—web application for generating input files for ORCA molecular modelling package made with the Anvil platform. Mol Simul. 2023;49(1):117–23. https://doi.org/10.1080/08927022.2022.2126865.
56. Shahraki S, Saeidifar M, Shiri F, Heidari A. Assessment of the interaction procedure between Pt (IV) prodrug [Pt (5,5′-dmbpy) Cl4 and human serum albumin: combination of spectroscopic and molecular modeling technique. J Biomol Struct Dyn. 2017;35(14):3098–106. https://doi.org/10.1080/07391102.2016.1243074.
57. Van Speybroeck V, Gani R, Meier RJ. The calculation of thermodynamic properties of molecules. Chem Soc Rev. 2010;39(5):1764–79. https://doi.org/10.1039/B809850F.
58. Basha FA, Khan FLA, Muthu S, Raja M. Computational evaluation on molecular structure (monomer, dimer), RDG, ELF, electronic (HOMO-LUMO, MEP) properties, and spectroscopic profiling of

8-Quinolinesulfonamide with molecular docking studies. Comput Theoret Chem. 2021;1198: 113169. https://doi.org/10.1016/j.comptc.2021.113169.
59. Gracia JC, Boto RA, Ruiz VI, Reva I, Woller T, Alonso M. A benchmark for the non-covalent interaction (NCI) index or…is it really all in the geometry? Theoret Chem Acc. 2016;135(10):1–14. https://doi.org/10.1007/s00214-016-1977-7.
60. Dexlin XDD, Tarika JDD, Kumar SM, Mariappan A, Beaula TJ. Synthesis and DFT computations on structural, electronic and vibrational spectra, RDG analysis and molecular docking of novel anti-COVID-19 molecule 3,5-dimethyl pyrazolium 3,5-dichloro salicylate. J Mol Struct. 2021;1246: 131165. https://doi.org/10.1016/j.molstruc.2021.131165.
61. Gupta S, Prakash A, Savita S, Hashmi K, Mishra P, Veg E, Khan T, Patel DK, Joshi S. Studies of some mixed ligand–metal complexes of 4-((2-(phenylcarbamothioyl) hydrazinylidene) methyl) benzoic acid in search of potential antimicrobial activity. J Mol Struct. 2024;1318: 139319. https://doi.org/10.1016/j.molstruc.2024.139319.
62. Suresh S, Ramanand A, Jayaraman D, Mani P. Review on theoretical aspect of nonlinear optics. Rev Adv Mater Sci. 2012;30(2):175–83.
63. Papadopoulos MG, Sadlej AJ, Leszczynski J. Non-linear optical properties of matter. Dordrecht: Springer; 2006. p. 1–676.
64. Kuzyk MG. Using fundamental principles to understand and optimize nonlinear-optical materials. J Mater Chem. 2009;19(40):7444–65. https://doi.org/10.1039/B907364G.
65. Jiang X, Kang L, Luo S, Gong P, Lee MH, Lin Z. Development of nonlinear optical materials promoted by density functional theory simulations. Int J Mod Phys B. 2014;28(27):1430018. https://doi.org/10.1142/S0217979214300187.
66. Shamina AH, Ganesan V, Jothy VB, Manikandan A, Muthu S, Javed S. Quantum chemical computations on molecular composition, spectroscopic properties, topology exploration, NLO, ligand protein interactions and pharmacokinetic evaluation of 8-hydroxyquinolium 3-nitrobenzoate. Chem Phys Impact. 2024;8: 100394. https://doi.org/10.1016/j.chphi.2023.100394.
67. Pooja K, Fatima A, Sharma A, Garima K, Savita S, Kumar M, Verma I, Siddiqui N, Javed S. Experimental, theoretical, hirschfeld surface, electronic excitation and molecular docking studies on fomepizole(4-methyl-1*H*-pyrazole). J Mol Struct. 2022;1256: 132549. https://doi.org/10.1016/j.molstruc.2022.132549.
68. Suresh A, Manikandan N, Jauhar RM, Murugakoothan P, Vinitha G. Growth and characterization of urea *p*-nitrophenol crystal: an organic nonlinear optical material for optoelectronic device application. Appl Phys A. 2018;124:1–10. https://doi.org/10.1007/s00339-018-1767-2.
69. Rafik A, Lakhdar F, Zouihri H, Guedira T, Acharjee N, Islam MS, Salah M, Zeroual A. Experimental and theoretical study of hybrid dihydrogen phosphate system: insights into bulk growth, chemical etching, nonlinear optical properties, and antimicrobial activity. 2024. https://doi.org/10.21203/rs.3.rs-3921223/v1.
70. Garima K, Fatima A, Pooja K, Savita S, Sharma M, Kumar M, Muthu S, Siddiqui N, Javed S. Quantum computational, spectroscopic, hirshfeld surface analysis of 3-picoline (monomer and dimer) by DFT/TD-DFT with different solvents, molecular docking, and molecular dynamic studies. Polycyclic Arom Compd. 2023;43:7828–52. https://doi.org/10.1080/10406638.2022.2140681.
71. Zhang MQ, Wilkinson B. Drug discovery beyond the 'rule-of-five.' Curr Opin Biotechnol. 2007;18(6):478–88. https://doi.org/10.1016/j.copbio.2007.10.005.
72. Haritha M, Sreeraga M, Suresh CH. Quantifying the hydrogen-bond propensity of drugs and its relationship with Lipinski's rule of five. Interactions. 2024;15(16):24–8. https://doi.org/10.1039/D3NJ05476D.
73. Jenssen H. Anti herpes simplex virus activity of lactoferrin/lactoferricin–an example of antiviral activity of antimicrobial protein/peptide. Cell Mol Life Sci CMLS. 2005;62:3002–13. https://doi.org/10.1007/s00018-005-5228-7.
74. Jeon OC, Seo DH, Kim HS, Byun Y, Park JW. Oral delivery of zoledronic acid by non-covalent conjugation with lysine-deoxycholic acid: in vitro characterization and in vivo anti-osteoporotic efficacy in ovariectomized rats. Eur J Pharm Sci. 2016;82:1–10. https://doi.org/10.1016/j.ejps.2015.11.004.
75. Saikia S, Bordoloi M. Molecular docking: challenges, advances and its use in drug discovery perspective. Curr Drug Targets. 2019;20(5):501–21. https://doi.org/10.2174/1389450119666181022153016.
76. Meng XY, Zhang HX, Mezei M, Cui M. Molecular docking: a powerful approach for structure-based drug discovery. Curr Comput Aided Drug Des. 2011;7(2):146–57. https://doi.org/10.2174/157340911795677602.
77. Sharma V, Savita S, Patra GK. A highly sensitive triazole-based perfectly water soluble novel bis-Schiff base reversible fluorescent-colorimetric chemosensor for fast detection of Pb^{2+} ions. RSC Adv. 2024;14:3289–303. https://doi.org/10.1039/D3RA06185J.
78. Pettersen EF, Goddard TD, Huang CC, Couch GS, Greenblatt DM, Meng EC, Ferrin TE. UCSF Chimera—a visualization system for exploratory research and analysis. J Comput Chem. 2004;25:1605–12. https://doi.org/10.1002/jcc.20084.
79. Morris GM, Huey R, Olson AJ. Using autodock for ligand–receptor docking. Curr Protoc Bioinf. 2008;24(1):8–14. https://doi.org/10.1002/0471250953.bi0814s24.
80. Fang Y. Ligand–receptor interaction platforms and their applications for drug discovery. Expert Opin Drug Discov. 2012;7(10):969–88. https://doi.org/10.1517/17460441.2012.715631.

Publisher's Note